Residual Stress, Aging, and Fatigue Fracture in Injection Molded Glassy Polymers I. Polystyrene

A.V. IACOPI* and J.R. WHITE, *Department of Metallurgy and Engineering Materials, University of Newcastle upon Tyne, Newcastle upon Tyne, NE1 7RU, United Kingdom*

Synopsis

Fatigue tests have been conducted on polystyrene bars molded at different pressures and having different post-molding thermal histories. Fatigue crack propagation rates were not sensitive to molding or thermal history but in unnotched bars initiation seemed to happen more quickly in bars aged for long periods at room temperature or annealed at elevated temperature. Fractographic studies showed that initiation occurred at favored sites and that the skin/core morphology affected crack growth. Prolonged storage of polystyrene bars at −85°C promoted significant physical property changes (stiffness and density). These changes appeared to be at least partly reversible with rapid recovery occurring within the first 24 h after restoring to room temperature.

INTRODUCTION

Injection moldings contain residual stresses that are the result of differential cooling rates during solidification. Under conventional molding conditions the stresses are tensile in the interior and compressive near to the surface.[1] Annealing or aging at a uniform temperature normally causes a reduction in stress magnitude without reversing the sense of the stresses.[2,3] Special molding conditions can cause the formation of compressive residual stresses in the interior balanced by tensile stresses near to the surface.[4] Post-molding conditioning can also cause a reversal in the stress sense and has been observed with nylon-6 when heated in water.[5] Stress reversal near one face has been promoted in polystyrene (PS) and other polymers by subjecting moldings to a temperature gradient[6] (stress becoming tensile at the hotter face), and by weathering in a hot climate[7] (stress becoming tensile at the face exposed to direct sunlight). Residual stresses in unfilled polymeric components are often in the range 1–10 MN/m^2 and therefore of a magnitude which may be significant compared to the applied stress under service conditions.

Polymeric components often fail by fatigue fracture.[8] Fatigue fracture can occur at stress amplitudes much lower than the stress required to break a glassy polymer molding in a single application and the magnitude of residual stress, at least at some locations, is significant by comparison. It is therefore of importance to know whether residual stresses influence fatigue crack ini-

*Present address: Plessey Semiconductors Ltd., Tamerton Road, Roborough, Plymouth, Devon, U.K.

Journal of Applied Polymer Science, Vol. 33, 577–606 (1987)

CCC 0021-8995/87/020577-30$04.00

tiation and/or propagation and the studies described here were conducted primarily to investigate this. Specimens with different residual stress distributions were prepared using a range of molding conditions and post-molding conditioning procedures. Notched specimens were used to obtain crack propagation data, but unnotched specimens were also tested to obtain information on the process of fatigue crack initiation.

EXPERIMENTAL

Specimen Production and Storage

Specimens were molded from BP KLP35/SC general purpose PS with the ASTM D638 type I dumbbell profile and measured approximately 190 mm long and 12.7 × 3.1 mm across the gauge length. They were made on a Butler-Smith 100/60 machine with a single end-gated cavity using conditions given in Table I.

A large fraction of the specimens made during each molding run were to be placed in a cold storage cabinet held at −85°C. The intention was to attempt to suspend the material in the as-molded condition so that tests could be conducted over an extended period of time on specimens that had been made in the same molding run and were therefore nominally identical. Aging trials would then be characterized by the time at room temperature after removing the bar from the cold storage cabinet and allowing it to warm to room temperature. (Checks were made periodically to test the hypothesis that the as-molded state would be "frozen-in" at −85°C and the results, which revealed a rather complicated response to this procedure, will be discussed later). In order to fulfill the requirement that each specimen had a similar thermal history, it was necessary to cool the specimens similarly. If the test bars were simply allowed to cool in air and then placed in batches into the cold storage cabinet, each specimen would have a different room temperature aging time prior to the second stage cooling, covering a fairly large range (e.g., up to 100 machine cycles, of the order of 100 min). To overcome this problem, the following routine was adopted: Specimens were taken from the molding machine, numbered for identification, and placed on edge on the bench to cool in air. Immediately after removing the 15th specimen from the molding machine, the first one was transferred to a plastic bag containing silica gel and surrounded by crushed cardice. Each molding cycle another specimen was transferred into the "cold bag" so that each specimen was cooled in air for the same amount of time (between 14 and 15 machine cycles) before being cooled

TABLE I
Injection Molding Conditions

Temperatures (°C)		Injection pressure (single stage) (MPa)
Barrel: zone 1/zone 2/nozzle	Mold (both platens)	
170/230/150	35	62
170/230/150	35	124
170/230/150	35	186

to depressed temperature. The bags containing specimens (10/per bag) and silica gel were finally labelled and transferred to the cold storage cabinet set at −85°C.

Test pieces were permitted 30 min to warm up to room temperature after removal from the cold cabinet if tests were required in the "as-molded" state. As will be discussed later, the results obtained on specimens which had followed this thermal history showed that the as-molded condition was not preserved exactly by this procedure.

Specimen Conditioning

Specimens were tested after conditioning in various ways, as listed below.

A. As-molded and stored at −85°C.
B. Stored at −85°C and then aged at room temperature.
C. Stored at −85°C and then annealed at elevated temperature.
D. Stored at −85°C and then mechanically preconditioned by cyclic loading.

Annealing was conducted in a vacuum oven using specimens taken from the cold cabinet and allowed to equilibrate at room temperature for 20 min before inserting into the preheated oven. At the end of the annealing period, the power was switched off and the specimens were allowed to cool slowly in the oven overnight.

The purpose of mechanical preconditioning by cyclic loading was to investigate whether this process, which is inevitably suffered by a specimen during fatigue crack propagation, modifies the residual stress distribution. Were this to be so, then the crack would grow into a region containing stresses different to those in a similar location in a bar that had not been loaded in this manner, and stress distribution analysis conducted on such a bar would then be irrelevant. In the experiments conducted here, unnotched specimens were used and cycled at stress amplitudes that would be sufficient to promote fatigue crack propagation from a notch but which did not cause fracture over an extended period in the absence of a notch. Small crazelike defects appeared near to the surface during this process, and it seems likely that failure might have occurred had load cycling at this level been prolonged for a much longer period.

Residual Stress Measurement

Residual stresses were measured using the layer removal technique. Description of the procedure and discussion of the analysis of the data have been presented in detail elsewhere.[1,9] Briefly, the technique involves removing thin uniform layers from the test bars by high speed milling and measuring the curvature ρ (= 1/radius) of the bar in response to the imbalanced stresses at each removal. The plot of ρ vs. total depth of material removed $(z_0 - z_1)$ is then used to obtain the necessary data to apply a modified version of the formula derived by Treuting and Read[9,10]:

$$\sigma_i(z_1) = \frac{-E}{6(1-\nu^2)}\left[(z_0+z_1)^2\frac{d\rho}{dz_1} + 4(z_0+z_1)\rho - 2\int_{z_1}^{z_0}\rho\,dz\right]$$

E is the Young's modulus, taken here to be 2.2 GN/m^2, and ν the Poisson ratio, taken here to be 0.33. $\sigma_i(z_1)$ is the stress in the bar axis direction at a position z_1 measured from the plane which was located at the bar center prior to layer removals, the bar surfaces located at $z = \pm z_0$. This version of the Treuting and Read formula is suitable if the radius of curvature of the bar in the direction perpendicular to the axis is very large.[9] With narrow bars this is difficult to measure, and it was not possible to confirm the validity of this approximation, but other studies have shown that when flow is parallel to the bar axis the error is not great for injection moldings.[9]

Fatigue Tests

The fatigue rigs used in this study have been described in detail before.[11,12] Tests were conducted under conditions that were effectively stress-controlled. The drive unit has a constant amplitude, but the nondriven end of the specimen is attached to a crosshead that can be moved under the action of a servo motor. The load is monitored continuously using a Pye-Ether/Pioden UF2 bidirectional load cell and the maximum value is compared with the preselected value. If there is a mismatch, then a command is sent to the servo motor and the crosshead moves to restore the preselected maximum load. Thus, if there is no cyclic softening or hardening of the material, then under constant deformation amplitude the minimum load will retain the value set at the beginning also, and the displacement of the crosshead can be taken to equal the accumulated dynamic creep. Tests were conducted in tension with minimum load close to zero (minimum stress/maximum stress ≤ 0.1).

Tests were conducted at either 0.08 or 0.42 Hz. Neither frequency is high enough to produce general heating of the specimen through viscoelastic dissipation.

The specimen was placed in a constant temperature enclosure, held at 25°C, and for some of the tests this was connected to a constant humidity generator (MCM "Aquamatique") set to provide a relative humidity of 40%. Some tests were conducted at very different humidities; but, within the wide scatter of data, no effect of humidity could be detected, and measurements obtained at different humidities or without humidity control are not distinguished in the results presented below.

Unnotched specimens were tested to failure at various stress amplitudes to generate an S–N curve. Visual observations were made throughout the course of these tests to identify the position of craze nucleation and the pattern of craze growth.

Crack propagation data were recorded on specimens provided with a central edge notch. The notch was 0.5 mm deep with a 0.25 mm radius and was cut to very reproducible dimensions using a notch cutting apparatus (by Daventest) designed to provide standardised notches in Izod test bars using a broach with 56 blades. The crack was photographed at intervals using a 35 mm camera with a 90 mm lens and extension tube providing a slight enlargement on the negative. The camera was fitted with a motor driven film advance and could be set for automatic operation permitting unsupervised testing. The camera was triggered using a two gated arrangement, the first gate opening after a preset interval using a home-built timing device and the second gate opening

under the action of a microswitch activated directly by the main drive unit. The microswitch could be set to operate at any chosen phase of the deformation cycle and was normally placed at the maximum tension position because it was found that the crack was photographed with greatest visibility when in this attitude. A synchronization arrangement such as this is necessary because the apparent crack length varies during the deformation cycle. A cycle counter was placed adjacent to the crack in the specimen and was included in the photograph frame. Thus, the exact cycle number was recorded each time and did not have to be derived from the preset time interval. A further advantage was that no error could be made in identifying each exposure in a sequence; this was especially valuable when the film was cut for storage. The crack length was measured directly from the negative using a travelling microscope.

The crack growth rate, dc/dN, was obtained at different values of c, the crack length, from plots of c vs. N, the number of cycles. The results are presented as plots of log dc/dN vs. log ΔK, where ΔK is the stress intensity factor range.[8] ($\Delta K = \Delta\sigma Y c^{1/2}$, where $\Delta\sigma$ is the stress range and Y is a geometric factor.)

Birefringence Measurements

The relative retardation was measured by viewing the specimen between crossed polars and identifying the characteristic color corresponding to the optical path difference caused by the double refraction of polychromatic light in the specimen. The birefringence varies throughout an injection-molded bar, changing very rapidly through the thickness (z-direction). In some parts of the bar, birefringence changes very slowly in the x–y plane and a location 80 mm from the gate was chosen to compare the average (through thickness) birefringence for bars in different states. Some readings were taken during cyclic loading tests, at both the maximum and minimum stress positions. In other experiments the relative retardation was measured in the unloaded state, either immediately after unloading or after an extended period under zero applied load.

Tensile Tests

Tensile tests were carried out using a J-J Instruments T5003 machine operated with a crosshead speed of 10 mm/min, chosen because this gives a strain rate similar to the average strain rate during the cyclic loading tests. In the absence of a satisfactory extensometer for use with our specimens, results were recorded as load–crosshead displacement curves. At least three tests were conducted on each type of specimen and reproducibility was extremely good.

Scanning Electron Microscopy

Fracture surfaces were gold-coated and examined in the scanning electron microscope (SEM) using the secondary electron image. Examples of fatigue-fractured specimens (both notched and unnotched) and samples broken in uniaxial tensile tests were inspected.

Density Measurements

A density column was used to measure densities from samples machined from the skin and core of moldings in different states. In some cases values were recorded over an extended period, and it was found that for some specimens the density changed significantly. Separate experiments were conducted to determine whether this effect was a consequence of the immersion of the specimen in the aqueous column (through swelling or some other interaction). Specimens aged in the column and specimens of the same type aged at the same temperature and for the same time in air before introducing into the column were found to give identical results, and it is concluded that the time-dependent density changes reported below reflect a genuine aging effect.

The skin and core were found to have quite different densities, confirming theoretical predictions and the experimental results obtained by others.[13] An attempt was made in addition to determine to what extent the density varies across the width of the specimen within the core region. To do this the skin was machined away from the xy faces (top and bottom) leaving core material through the whole of the thickness (z-dimension) of the remainder except at the edges [Fig. 1(a)]. A series of specimens of different widths (y) between 5 mm (just less than half of the full bar width) up to the total bar width were prepared by cutting away from one edge only [Fig. 1(b)]. Each piece was given a characteristic marking and dropped into the column. The height of each specimen in the column was recorded at intervals, and the corresponding density value was plotted as average density p_{av} vs. thickness y. The density at a chosen location could then be estimated using the following derivation:

Let the volume of the specimen be V. Hence we can write expression for the mass as

$$p_{av}V = \int_0^{\Delta z}\int_0^{y}\int_0^{\Delta x} p\,(x, y, z)\,dx\,dy\,dz \tag{1}$$

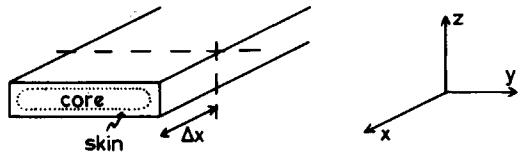

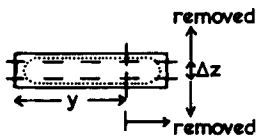

Fig. 1. Schematic of sectioning procedure: (a) section through the bar showing the parting of a sample measuring Δx along the bar axis (x-direction); (b) removal of the skin to leave the central Δz in the thickness (z-direction) and removal of one end of the remainder to leave a specimen of width y.

where $p(x, y, z)$ gives the density variation throughout the specimen. For a rectangular parallelipiped width y, thickness Δz, and length Δx, we have

$$p_{av} y \Delta x \Delta z = \int_0^{\Delta z} \int_0^{y} \int_0^{\Delta x} p(x, y, z)\, dx\, dy\, dz \tag{2}$$

It is not expected that the density variation will be very rapid in the bar axis (x −) direction, and so for short specimens as used here ($\Delta x \leq 4$ mm) it will be assumed that the density does not vary in the x-direction. If in addition it is assumed that the y and z density variations are independent (separable), then eq. (2) becomes

$$p_{av} y \Delta x \Delta z = \Delta x \int_0^{\Delta z} f(z)\, dz \int_0^{y} p(y)\, dy \tag{3}$$

By setting $\int_0^{\Delta z} f(z)\, dz = \Delta z$, we define $p(y)$ as the average through depth density at position y, and eq. (3) becomes

$$p_{av} y = \int_0^{y} p(y)\, dy \tag{4}$$

Differentiating both sides with respect to y, we obtain

$$p_{av} + y \frac{dp_{av}}{dy} = p(y) \tag{5}$$

dp_{av}/dy is obtained from the $p_{av}(y)$ plot and substituted into eq. (5) to obtain $p(y)$ at selected positions y.

RESULTS

Residual Stress Distributions

Residual stress distributions for bars molded at 62, 124, and 186 MPa machine pressures, respectively, are shown in Figures 2–4. In each case

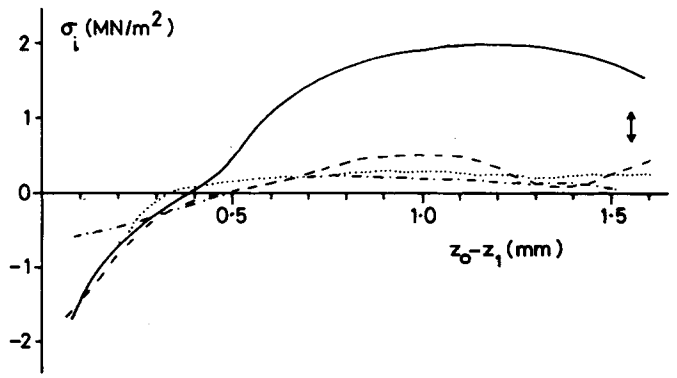

Fig. 2. Residual stress distributions in PS bars molded with 62 MPa injection pressure and conditioned in different ways (see text): (——) A; (· · ·) B; (·-·) C; (– – –) D.

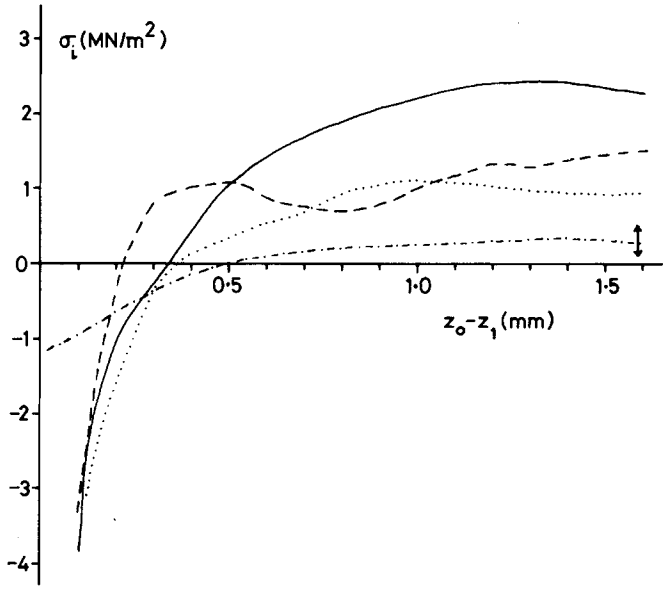

Fig. 3. Residual stress distributions in PS bars molded with 124 MPa injection pressure and conditioned in different ways (see text): (——) A; (· · ·) B; (-·-) C; (– – –) D.

analyses are presented for specimens in the following conditions:

A. Stored at −85°C and tested as soon as room temperature equilibrium was reestablished.
B. Stored at −85°C, and then aged for 16 h at room temperature.
C. Stored at −85°C and then annealed 5.25 h at 82°C and then slow cooled in the oven.
D. Stored at −85°C and then cyclically loaded at room temperature with $\Delta\sigma$ = 8 MN/m^2 for 16 h.

For bars molded at 62 and 124 MPa the highest stresses were recorded for specimens of type A and the lowest for type C. Type C (annealed) specimens gave the lowest stresses for bars molded at 186 MPa also. Type A specimens molded at 186 MPa gave the highest tensile residual stress measurements, but the analyzed residual stress profile is anomalous because of gross inequality of the areas under the tensile and compressive parts of the curve respectively. For a self-stressed bar with a symmetrical stress distribution, these should be equal. It has been shown[14] that if the assumptions made in the Treuting and Read analysis are violated (e.g., if Young's modulus is different in the skin and in the core of the injection molding instead of uniform throughout as assumed in the analysis), then the areas may differ, but it is unlikely that an inequality as large as that seen in Figure 4 can be explained in this way. The data from the repeated test show that this effect is not the consequence of measurement error, and we speculate that it is a result of rapid aging in the immediate period after reaching room temperature, i.e., during the time that the layer

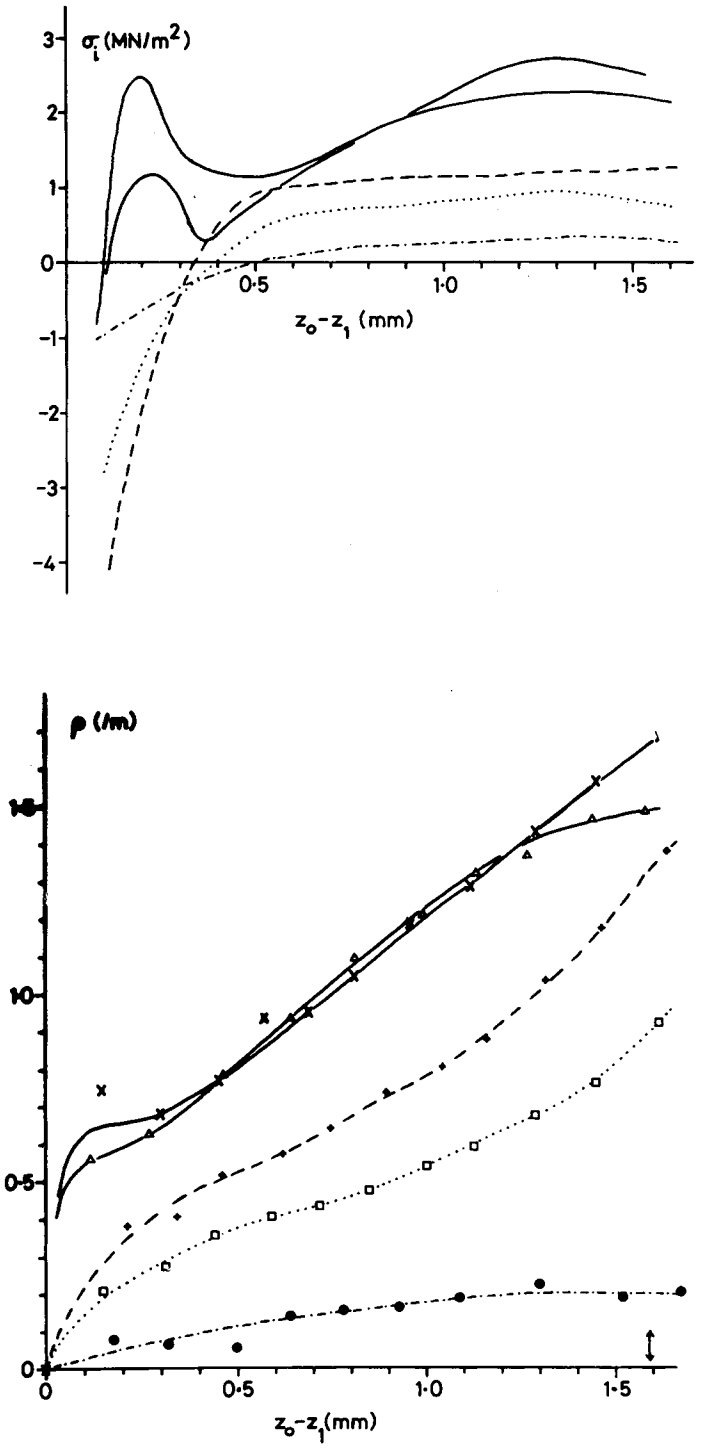

Fig. 4. (a) Residual stress distributions in PS bars molded with 186 MPa injection pressure and conditioned in different ways (see text): (——) A; (· · ·) B; (-·-) C; (– – –) D. (b) Curvature plots corresponding to the residual stress analyses in (a).

removal procedure was conducted, a process taking ~ 3 h.[†] That significant aging takes place during this period is confirmed by measurements of density, presented below. It follows that the results obtained for specimens of type A from the batches molded at 62 and 124 MPa must also be treated with caution, and this may be the reason why the analyzed residual stress distributions depart significantly from the parabolic profile predicted by simple theoretical treatments (compare with those obtained for PS in an earlier investigation[15]). Although it is not shown in Figure 4, the residual compressive stress very close to the surface in type A specimens was of greater magnitude than that observed with the other specimens molded at 186 MPa. This can be deduced from the fact that the curvature obtained after the first layer removal was much greater than that obtained with the other specimens. Exact location of the residual stress level within the first measurement interval cannot, of course, be attempted.

Specimens in which the residual stress distribution was determined 16 h after removing from cold storage showed stress levels intermediate between those obtained with specimens newly removed from cold storage and those obtained with annealed specimens. This was true for specimens molded at all three of the molding pressures used, and in each case the specimen which was cyclically loaded during this 16 h period showed stress levels of slightly higher magnitude than those in specimens aged at room temperature under no applied load.

Fatigue Behavior

***S–N* Curve.** Specimens molded at 124 MPa and stored at −85°C were used to determine a reference *S–N* curve, using unnotched samples cycled at 0.08 and at 0.42 Hz. The results are plotted on Figure 5 and do not seem to be very sensitive to frequency. Results from tests on specimens molded at 62 and 186 MPa are also shown, and these fall close to the same curve. Specimens that have been annealed at 82°C or aged at room temperature for 30 months show a significant drop in fatigue resistance (Fig. 5).

Crack Propagation Analysis. Crack propagation data corresponding to specimens molded at all three pressures and tested after storage at −85°C, but with no further aging are shown in Figure 6. There is significant scatter, though note that this has been emphasized by using a ΔK axis that is more expanded than is commonly found in the literature. In the presence of the scatter it is not possible to find any indication of differences in crack propagation behavior that can be related to molding pressure. Results from annealed specimens are also shown and fall within the scatter band defined by specimens stored at −85°C and not aged at room temperature nor at elevated temperature.

[†]The problem of relaxation of residual stress during the execution of the layer removal procedure has been addressed before.[6] Even with a well-equilibriated specimen, the removal of a layer produces a new stress distribution which will trigger some stress relaxation, but the effect is usually modest. In exceptional cases, such as type A specimens, a modified or alternative method of residual stress assessment is required.

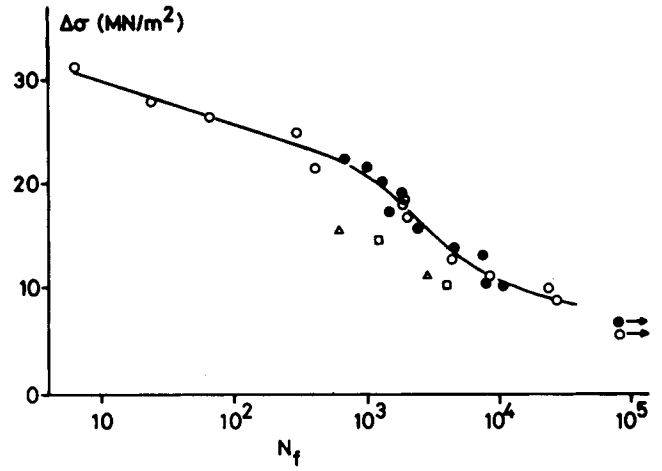

Fig. 5. S–N curve for PS unnotched bars cycled at 0.08 Hz (open symbols) and 0.42 Hz (solid symbols). Results for specimens annealed for 5 h at 82°C (△) and aged for 30 months at room temperature (□) are included.

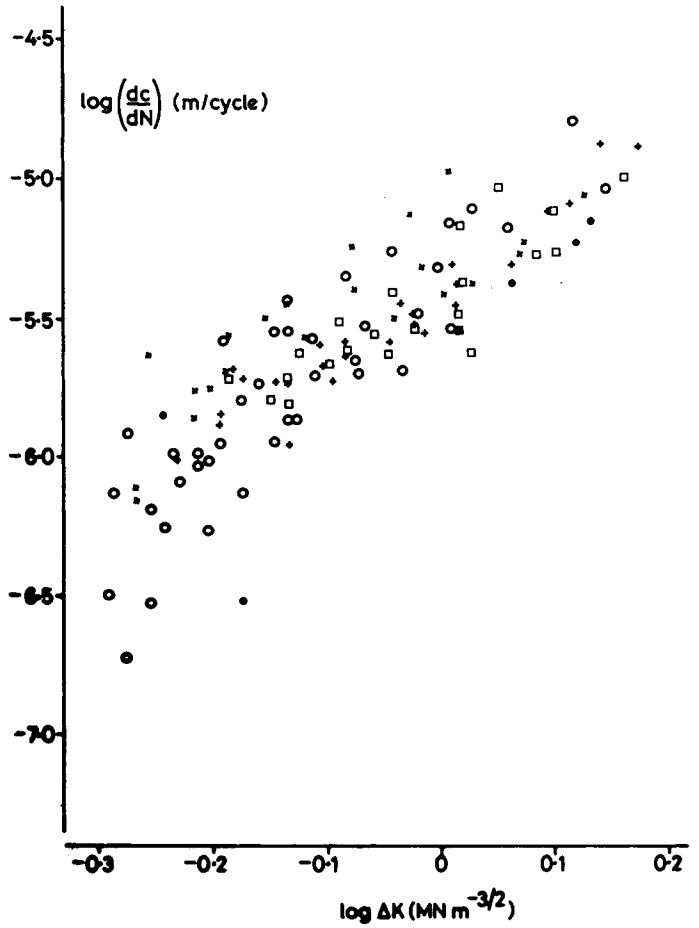

Fig. 6. Crack propagation rate plotted vs stress intensity factor range (ΔK). Included are data from bars molded with injection pressure: (+) 62 MPa; (○) 124 MPa; (×) 186 MPa; (□) annealed specimens.

Birefringence

PS possesses a positive stress optical coefficient, but if orientation is produced by a tensile deformation either in the solid form or in the melt (then frozen-in by rapidly cooling), negative birefringence develops. It is frozen-in molecular orientation that causes most regions of injection-molded PS bars to show negative birefringence. In tensile stress–relaxation the deformation causes an immediate stress optical response, giving a positive increment to birefringence, then, as the stress relaxes, the birefringence changes more rapidly in the negative sense than can be accounted for by the reduction in stress alone.[16] This effect is shown in Figure 7 for one of the specimens molded at 124 MPa and monitored at a site 80 mm from the gate. Parallel curves, slightly displaced parallel to the Δn axis, were obtained at positions 100 and 120 mm from the gate. Unloading gave a further negative increment, corresponding to the short time stress optical effect. The extra time-dependent negative increment in birefringence that develops during the test is believed to be a consequence of alignment of the phenyl groups perpendicular to the tensile axis, possibly as a secondary effect of the alignment of main chain segments more parallel to the tensile axis.

Birefringence measurements made on PS during cyclic loading tests conducted at three different stress amplitudes are shown in Figure 8. Readings were taken at the point of maximum stress. It is evident that the highest stress range produced the most rapid change in birefringence. The initial separation of the birefringence curves is a consequence of the stress optical effect, and the specimen tested at the highest stress therefore has the highest

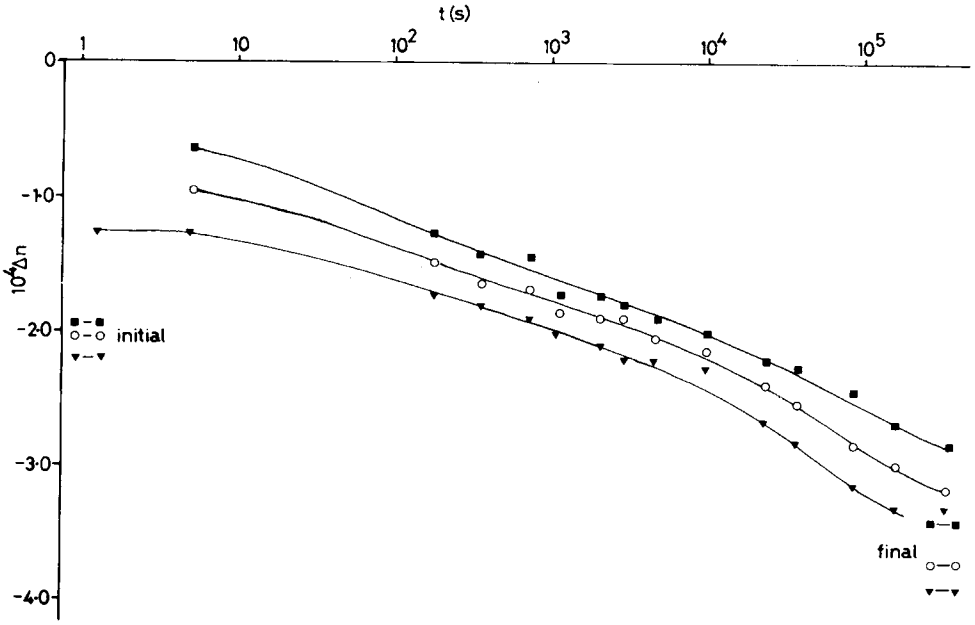

Fig. 7. Birefringence as a function of time during stress relaxation, showing measurements taken at three sites: (▼) 80 mm from the gate; (○) 100 mm from the gate; (■) 120 mm from the gate. Also shown are the values obtained at these positions prior to loading ("initial") and after unloading at the end of the stress relaxation test ("final").

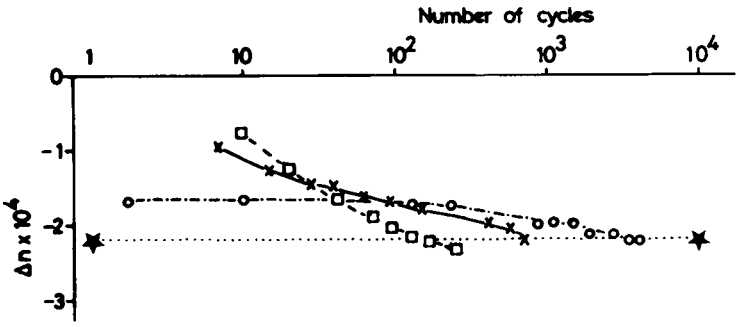

Fig. 8. Birefringence as a function of time during cyclic loading tests at peak stresses: (□) 19.3 MN/m^2; (×) 17.1 MN/m^2; (○) 8.8 MN/m^2. Measurements were taken at the peak load position. The value of birefringence in the unloaded bar prior to testing is shown for reference (★ · · · ★).

value; but the negative increment caused by the progressive development of orientation soon exceeds the stress optical separation, and the birefringence curves cross each other. It should be noted that the ultimate value of birefringence is determined not only by the stress amplitude but also by the number of cycles before failure, N_f. Figure 9 shows the birefringence recorded after the completion of tests on unnotched samples run to failure, plotted against N_f. These measurements were recorded several days after completing the tests and are free from short term recovery effects. In the middle range the time factor is dominant with the magnitude of the birefringence change increasing with N_f (and therefore decreasing with increasing stress range, $\Delta\sigma$).

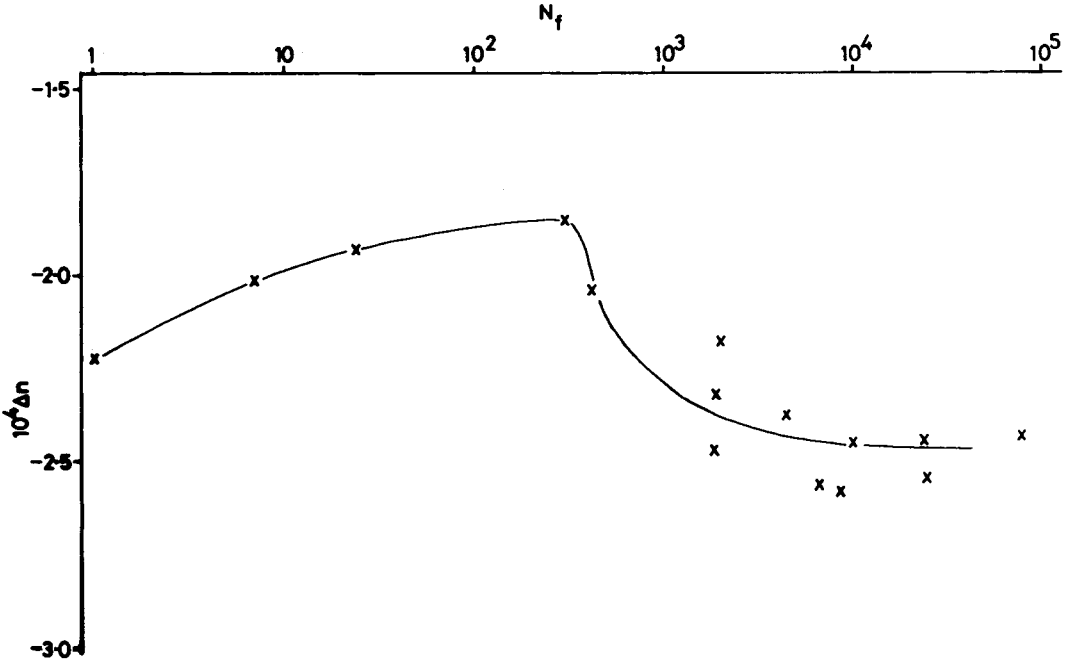

Fig. 9. Birefringence measured in the unloaded state in unnotched bars cyclically loaded to failure, plotted vs. the number of cycles to failure.

At low N_f (high $\Delta\sigma$) values, this trend is reversed, with the magnitude of the ultimate birefringence change decreasing with increasing N_f, whereas at the high N_f (low $\Delta\sigma$) end the ultimate birefringence appears to approach a constant value.

Tensile Tests

Figure 10 shows load–deformation curves for PS molded at 186 MPa and tested in the following conditions:

(a) stored 19 months at −85°C and tested as soon as room temperature equilibrium was restored;
(b) tested within 30 min of molding;

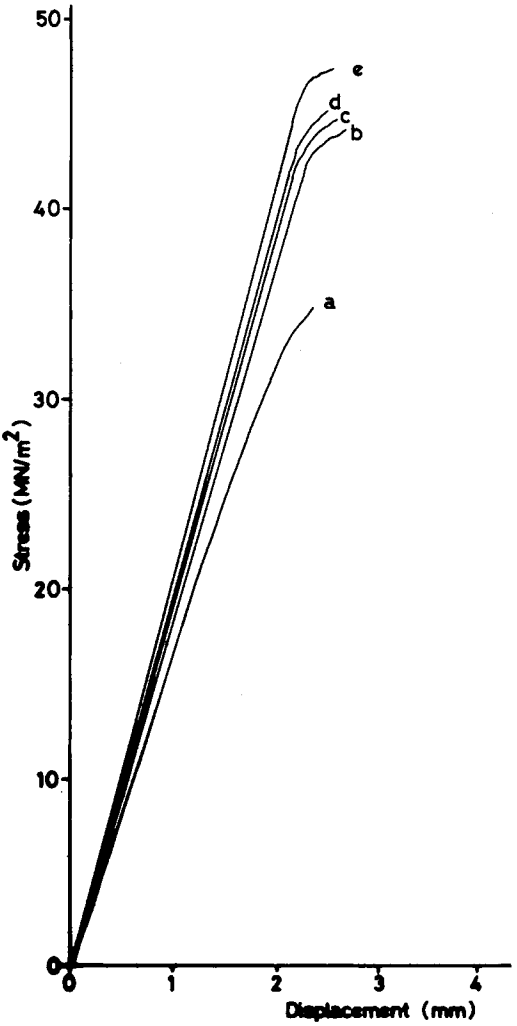

Fig. 10. Load–deformation curves for PS molded with 186 MPa injection pressure and conditioned in different ways a–e (see text).

(c) aged 4 days at room temperature (and never cooled to −85°C);
(d) aged 17 days at room temperature (and never cooled to −85°C);
(e) stored 19 months at room temperature.

Five specimens were tested in each of the conditions (b), (c), (d), three in condition (a), and two in condition (e). Very good reproducibility was obtained within each batch with no detectable variation in the nearly straight initial portion that persists until over 90% of the ultimate tensile stress was reached. From visual observation it was established that the sudden change in slope at the end of this portion coincided with the onset of crazing. A small variation in "ultimate tensile stress" (UTS) was observed between similar specimens. Aging at room temperature is shown to cause an increase in both stiffness and UTS of the PS specimens, whereas storage at −85°C has caused a decrease in both stiffness and strength. Similar results were obtained on specimens molded at 124 MPa.[17] Specimens stored at −85°C for shorter times were also tested and Figure 11 shows that the changes that occur at this temperature take a significant time to develop. Indeed a modest increase in the UTS is initiated at short times, and the UTS is still higher than the as-molded value after more than 2 weeks storage at −85°C, but then begins to decrease steadily. The initial behavior gave encouragement to the original expectation that no changes would occur at −85°C, and it is fortunate that further checks were made that revealed the long term behavior.

Some further experiments were conducted in which specimens which had been stored for 19 months (580 days) at −85°C were allowed to warm to room temperature then were subjected to a mechanical conditioning procedure for 16 h; some samples were cyclically loaded in tension with $\Delta\sigma = 8$ MN/m^2 (as the cyclically preconditioned samples used in the fatigue studies) whereas others were subjected to a stress–relaxation test with an initial stress of 20 MN/m^2. These specimens were then subjected to a tensile test, and in both

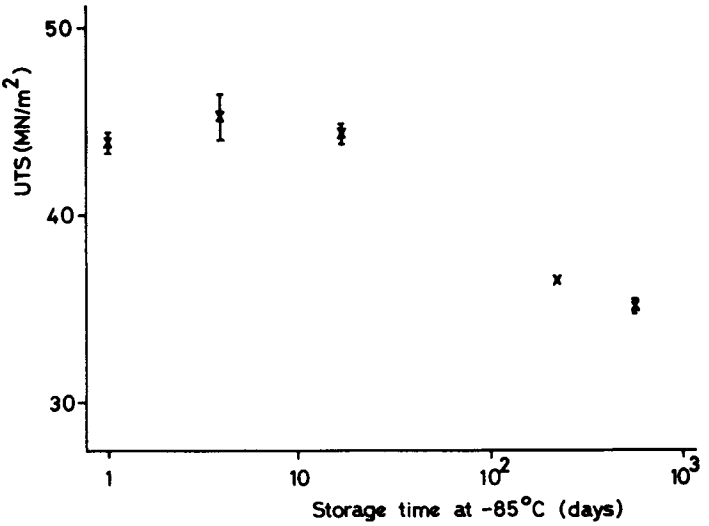

Fig. 11. "Ultimate tensile stress" (UTS) for specimens stored at −85°C for various periods of time.

cases a significant drop in the UTS was recorded compared to that obtained with samples aged at room temperature for 16 h with no applied load.[17] During the period of stress–relaxation, several small crazes developed at corner sites along the edge which on close examination showed some microscopic traces of flashing. Failure in the tensile test occurred from crazes which grew from these initial crazes at stresses lower than those required for general crazing to be produced.

VISUAL OBSERVATIONS AND SCANNING ELECTRON MICROSCOPY

The crazing pattern that developed during tensile testing was different for specimens in different states. Examples from moldings made at 124 MPa are shown in Figure 12. The specimen aged at room temperature for 8 months before testing has crazes with a coarse appearance stretching typically across half of the width of the bar, whereas the specimens which were stored at −85°C have coarse crazes near the edges but a dense pattern of fine crazes in the central region, occupying more than half of the bar. The specimen tested as soon as it was restored to room temperature appeared very similar to the one aged at room temperature for a further 16 h. Crazes first appeared near (but not at) the edge. In the case of samples aged at room temperature the crazes proceeded to grow inward towards the center. Specimens stored at −85°C then tested at room temperature after aging either for a few minutes only or for 16 h formed crazes in the interior before the initial coarse crazes reached that far (Fig. 13).

SEM inspection of the fracture surfaces from unnotched samples provided information that correlated well with the visual observations. The position at which craze nucleation took place was usually indicated. In the case of unnotched samples cyclically loaded to failure at relatively high strain amplitudes, the craze nucleus was found to be 1–2 mm from the edge of the specimen and had radial markings surrounding it (Figs. 14 and 15). Figures 14(a) and (b) show two initiation sites found on the same fracture surface, one at either end of the bar section [Fig. 14 (c)]. This confirms that crazes

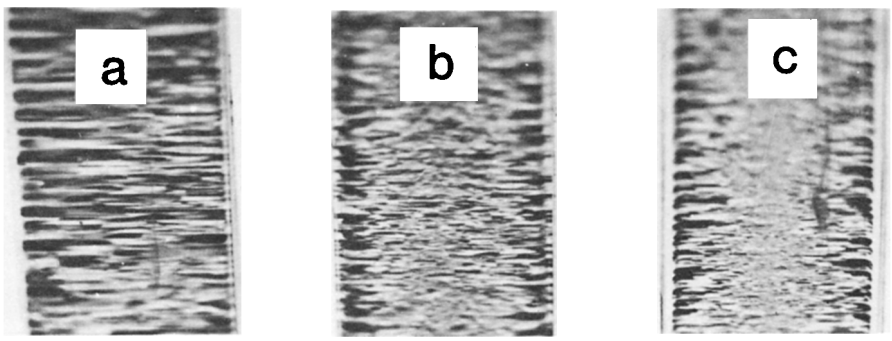

Fig. 12. Crazing patterns in bars molded at 124 MPa. The bars are viewed along the z-direction after tensile testing: (a) aged at room temperature for 8 months; (b) aged 16 h at room temperature after prolonged storage at −85°C; (c) tested as soon as room temperature equilibrium was restored after prolonged storage at −85°C.

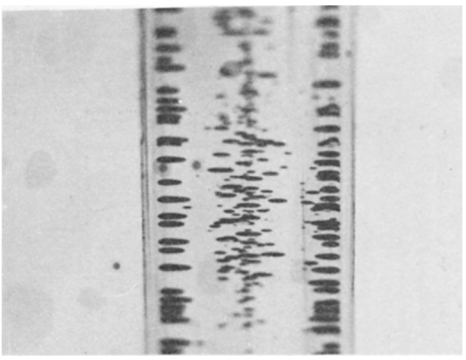

Fig. 13. Crazing pattern at an earlier stage of development in a bar tested in uniaxial tension at room temperature after prolonged storage at −85°C.

nucleated near both edges of the specimen then grew toward the center, and that the crack which caused failure united crazes growing in both halves of the specimen. Therefore, the less likely alternative that the crack began within a craze in one half of the bar and then grew through previously uncrazed material in the other half can be discounted. A flaw, possibly a small foreign particle, appears to have nucleated the craze in both of the examples shown in Figure 14, but cases in which no foreign particle or flaw of significant size was visible in the craze nucleation region were also common (e.g., Fig. 15). A distinct change in the fracture surface morphology was seen near the edge of the specimen, measuring nearly 0.4 mm in the specimen shown in Figure 15.

At low strain amplitudes crazes were found to nucleate near corners (as noted above in the discussion of bars mechanically preconditioned by cyclically loading prior to uniaxial tensile testing), and failure ultimately occurred by crack growth beginning in one of these corner defects. The fracture surface obtained with a specimen cycled to failure at low strain amplitude illustrates this (Fig. 16). A small flash remnant is visible at the corner in which the craze/crack nucleated. Prominent bands are in evidence on this specimen, radiating out from the nucleus. The spacing of these bands is similar to that found in the hackle region of a PS fracture surface,[18,19] but the surface is smoother. On the other hand, the bands are more widely spaced and contain rougher regions than is normally found with discontinuous growth bands.[8,20,21]

A clear indication of the site of craze nucleation was normally found with notched specimens too. Figure 17 shows that this could happen near to the center of the notch or fairly close to a corner. The bands show that the crack front can be markedly curved and that the progress of the crack can be quite different from one specimen to another. This emphasizes the problem encountered when attempting to locate the crack front for crack growth rate measurements. The crack is normally viewed at the surface, and, because of the small depth of field of the observing system, it is unlikely that more than about 0.5 mm of the crack front provides sharp contrast and therefore influences the reading. Variations in crack front position within this depth probably cause some blurring of the image, which is further degraded by contributions from deeper within the specimen. The crack front may have advanced to quite different positions at other depths within the bar, and it

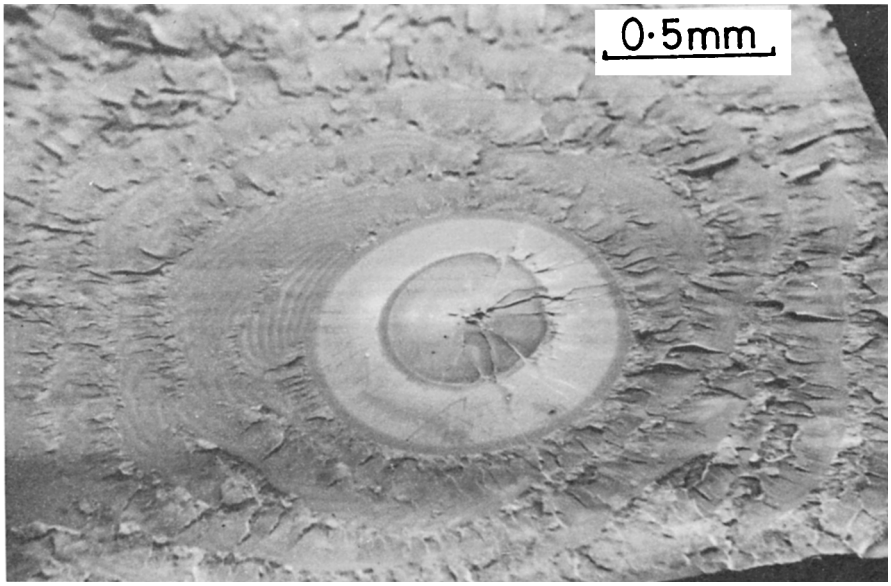

(a)

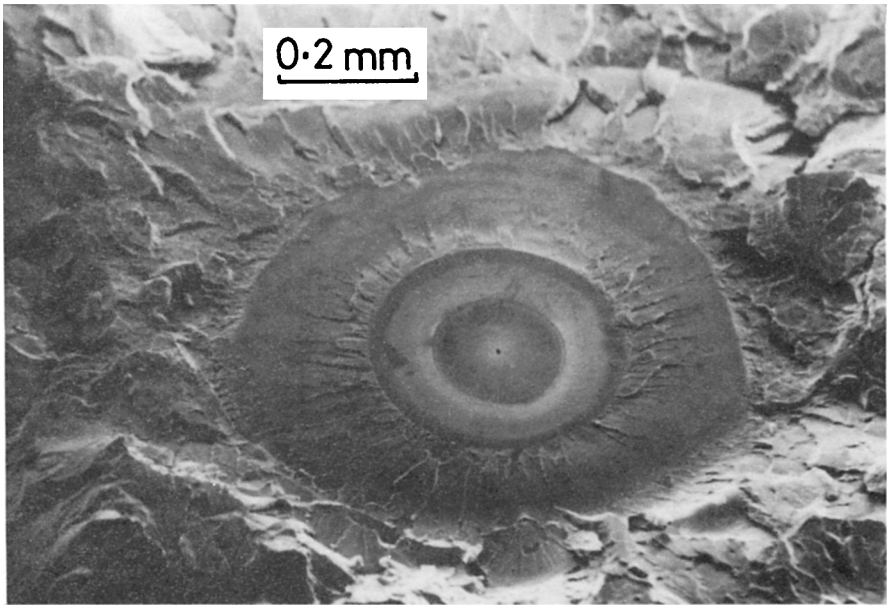

(b)

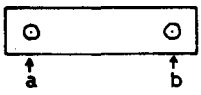

(c)

Fig. 14. Fatigue fracture surface obtained using a high strain amplitude; (a), (b) initiation sites of crazes which grew independently on either side of the specimen; cracks eventually grew through these crazes and met to form the fracture surface; (c) schematic showing the approximate locations of the areas shown in (a) and (b).

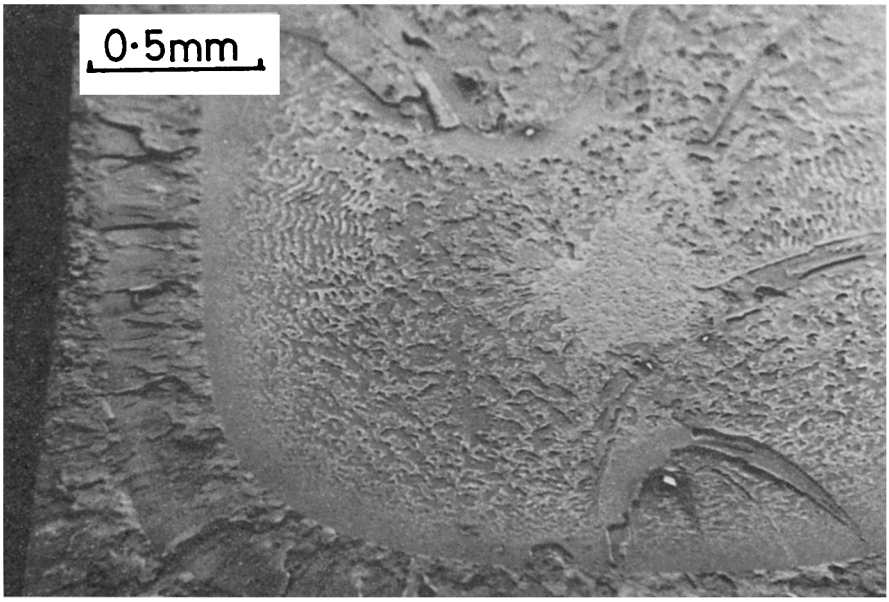

Fig. 15. Initiation site on a fatigue fracture surface. Note the sudden morphological change approximately 0.4 mm from the molded surface.

follows that a single measurement of crack length is not very satisfactory. Approximate calculations show that, for the amount of crack front curvature indicated by the fracture surface markings to be present in the specimens used in these tests, the error introduced by measuring the crack at the surface (and at one surface only) is sufficient to account for the scatter found in the crack

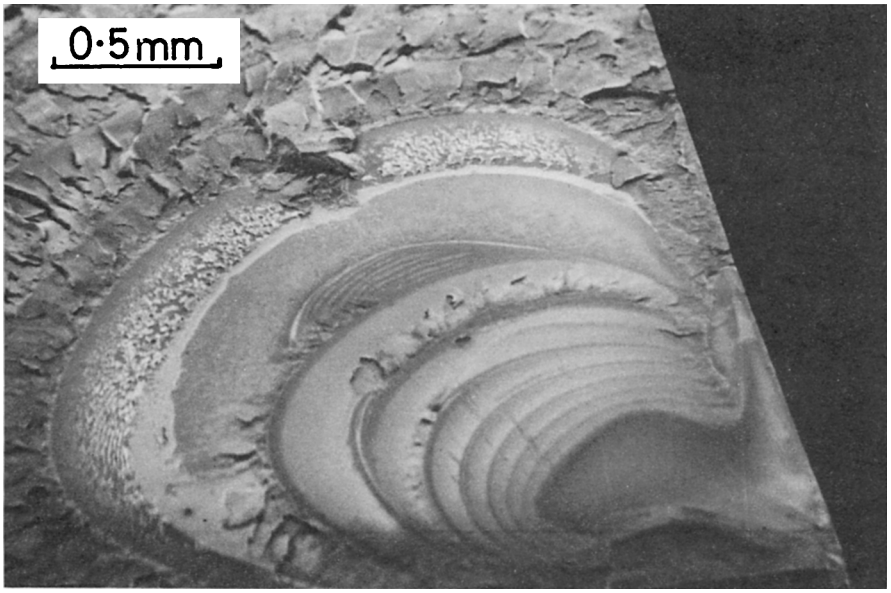

Fig. 16. Injection site on a fracture surface typical of low strain amplitude fatigue failure.

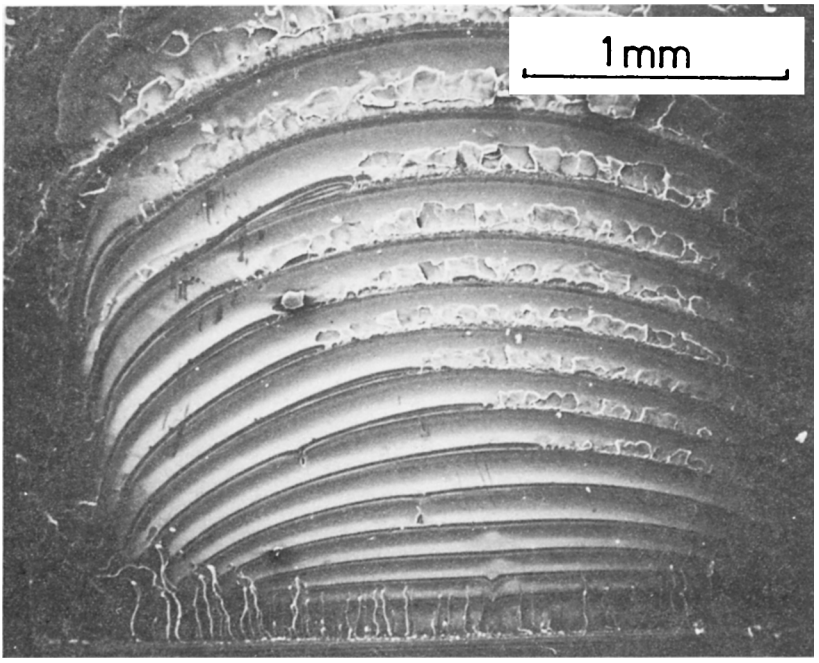

(a)

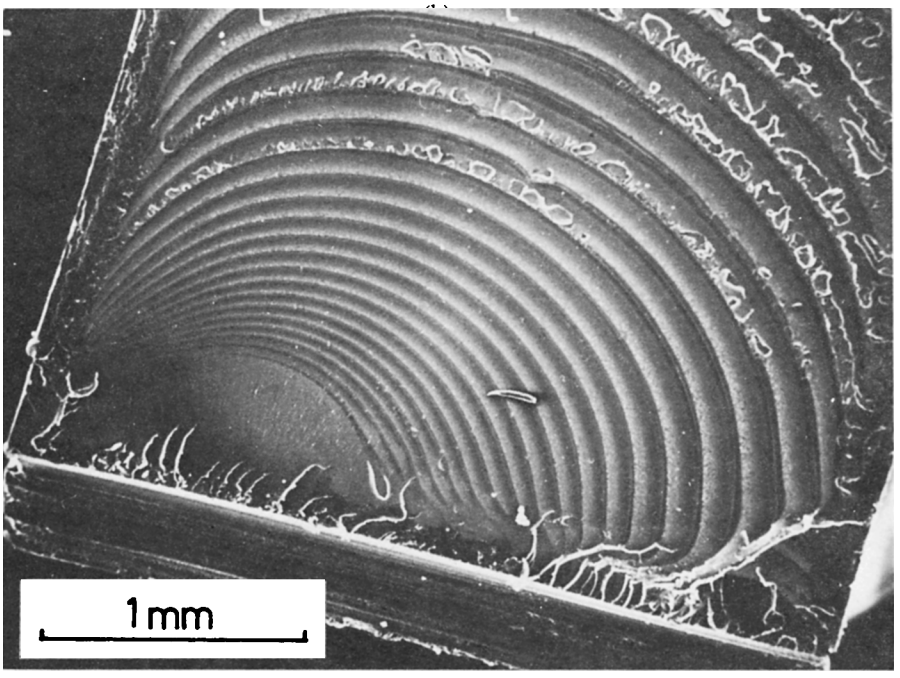

Fig. 17. Fracture surfaces from notched specimens illustrating initiation: (a) at the center of the bar; (b) near one corner.

growth data.[17] It is relevant to report here another visual observation made during the testing of notched samples. With some razor notched specimens failure was nucleated not at the notch but at a site opposite the notch and some distance from it. It is probable that multiple crazing promoted ahead of the razor blade caused local softening of the material, causing in turn the development of higher stresses at other positions ahead of the craze/crack.

The bands which commence at the notch and which were referred to above do not reach right to the surface of the specimen, and a thin strip of material was found near to the surface showing a different fracture morphology, as with the unnotched bars. This strip usually remained visible adjacent to the hackle region and was usually less than 0.4 mm thick, often much less, and remained of fairly uniform thickness within a particular specimen. If this morphology were the consequence of a central plane strain fracture zone, the surface region should get wider as the crack advanced.[8,22] On the other hand, the width of the surface zone differed from specimen to specimen even within a batch molded identically, indicating that the explanation cannot be simply found in the skin/core morphology of the moldings. It seems that there must be some influence exercised by the morphology, the fracture conditions, and, possibly, the residual stresses with the morphological effect being the strongest. Higher stress amplitudes generally produced a wider surface zone. As part of an investigation into the origin of the surface fracture feature, a sample was machined from both sides to leave the central 2 mm before testing. This removed ~ 0.5 mm on both sides, thus removing the injection molded "skin." With this specimen no prominent surface effect was observed on the fracture surface, and it was concluded that the near surface strip seen with the other specimens was probably not a shear lip (corresponding to a plane strain/plane stress transition[18,22-26]) because this should have been reproduced in the thinner sample, albeit in modified form. By removing 0.5 mm of surface on both sides, the remainder will consist of core material only, and will have very small residual stresses in the type of molding used for this experiment, for the residual stresses (prior to machining) changed steeply near the surface (in the region which was subsequently removed) and not very much at all in the 2 mm central region. Thus, there were no (strong) compressive stresses near to the surface to inhibit crack propagation, and this may be important in determining the fracture morphology. With specimens having large compressive residual stresses at the surface, crack propagation in this region may be postponed until the later stages in the test and may not occur until the final (fast) fracture takes place.

The nature of crazing in PS and the interpretation of the features seen on the fracture surfaces have been discussed extensively in the literature[8,18-21,27-29]; our observations have been in general agreement and will not be repeated here. Examples showing further details are found in Ref. 17. An example of a less common feature is shown in Figure 18 in which a mackerel pattern is found within one of the bands referred to above, just before the banded region gives way to a hackle pattern.

Density

First consider the results for the variation in density in the bar width (y-) direction. Figure 19 shows plots of p_{av} vs. y for a series of specimens of

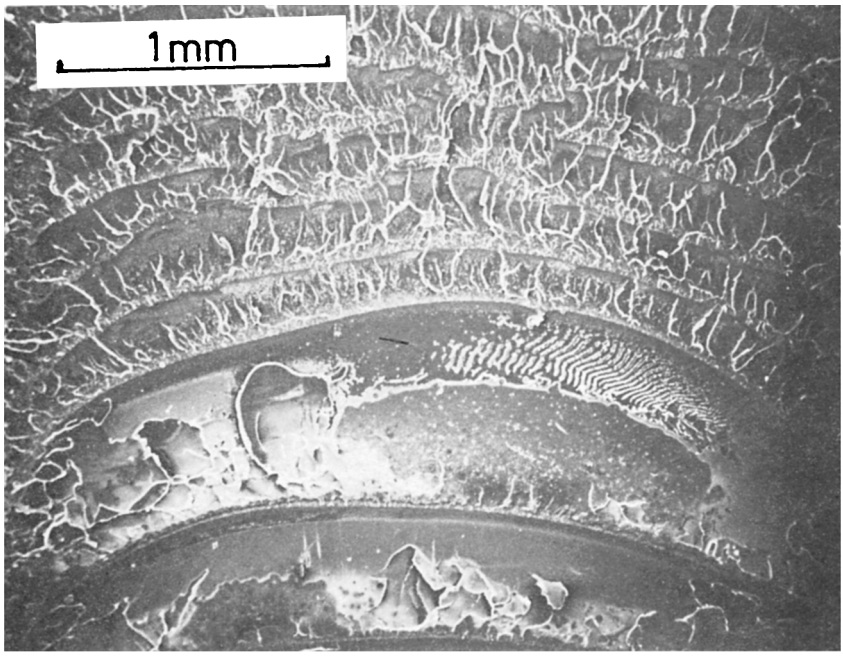

(a)

(b)

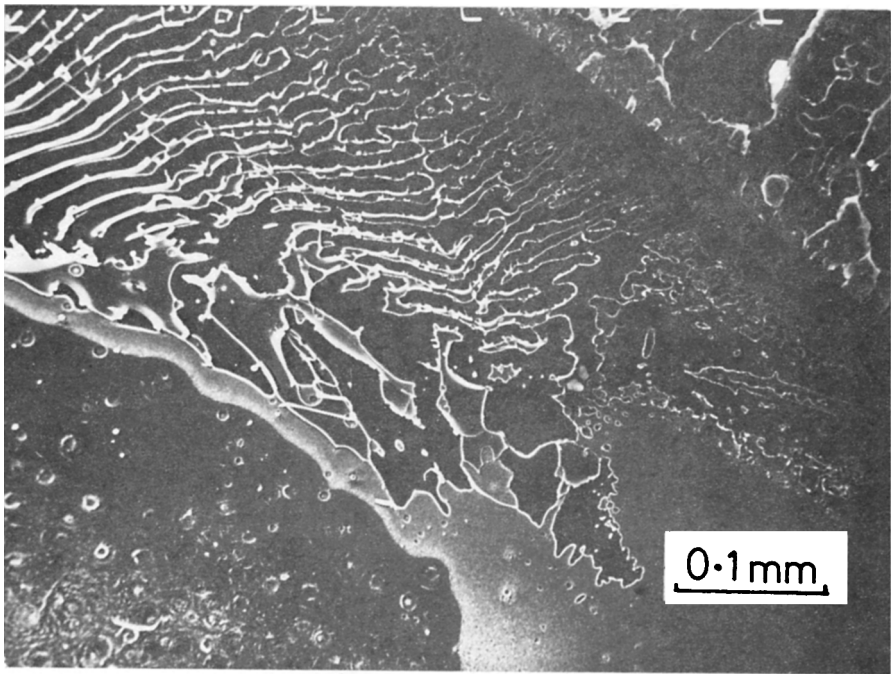

Fig. 18. Mackerel pattern within the last of the radial zones in the slow fracture region before the hackle region: (a) general view; (b) higher magnification image of the mackerel pattern.

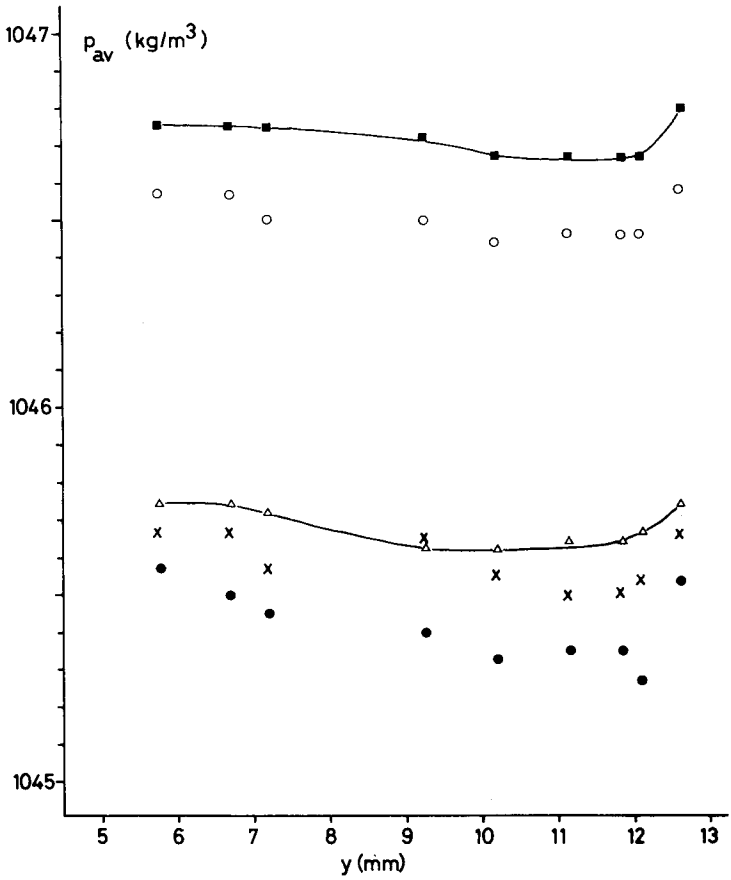

Fig. 19. Average density values recorded for specimens of different width y after the following times: (●) 20 min; (×) 135 min; (△) 315 min; (○) 7 days; (■) 13 days.

different widths y, deposited in the same column at the same time. These specimens were cut from near the center of bars which had been stored at $-85\,^{\circ}$C as described in Figure 1 and the accompanying text. Measurements were recorded at different times from 20 min up to 2 weeks, and a progressive densification was observed for all specimens. There is a slight tendency for the average densities to become closer to one another with aging. The curve obtained after 20 min shows the greatest density variation between the several specimens but is expected to contain the greatest measurement uncertainty. Therefore, the curves for 315 min and 13 days have been employed to obtain the $p(y)$ density–width profiles shown in Figure 20 using the method outlined in the Experimental section. The smoothed lines constructed on Figure 19 were used to represent p_{av} for this purpose. The $p(y)$ profile shows that the density in the core is almost constant (with respect to y) but rises sharply in the final millimetre nearest the surface (xz plane). Accurate estimates within this final measurement interval are not possible. The density may rise to higher values than those indicated in Figure 20, and the high density region may be confined to a strip narrower than 1 mm. These results

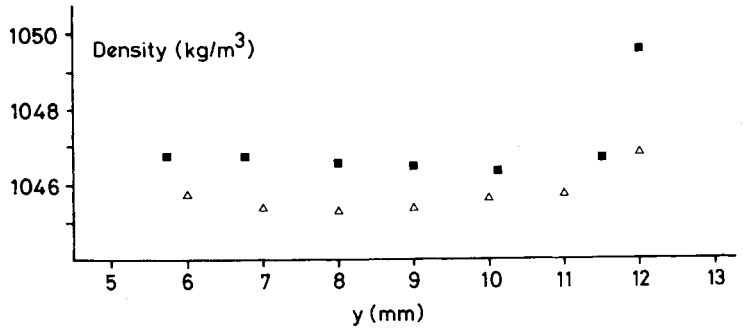

Fig. 20. Density versus position (y) profiles across the width of a 12.7 mm wide bar after 315 min (△) and 13 days (■).

indicate that, for studies of the depth dependence of density [$p(z)$], the width of the specimens (y dimension) could be fairly large as long as at least 1 mm was removed at each edge.

Skin samples machined from the xy face were found to have a higher density than core samples except when tested immediately after prolonged storage at $-85°C$. With PS bars aged at room temperature for 10 months, no variation in core density could be found within experimental error for samples taken at different locations along the bar axis and from bars molded at different pressures (1049.2–1049.3 kg/m^3). The skin densities were highest for the highest molding pressures, giving a range 1050.3–1051.5 kg/m^3, and with some samples the density at the end of the gauge length nearer to the gate end was slightly higher than that at the opposite end. These values stayed constant during a residence of 1 month in the column. Samples of skin and core material machined from newly molded bars were found to have much

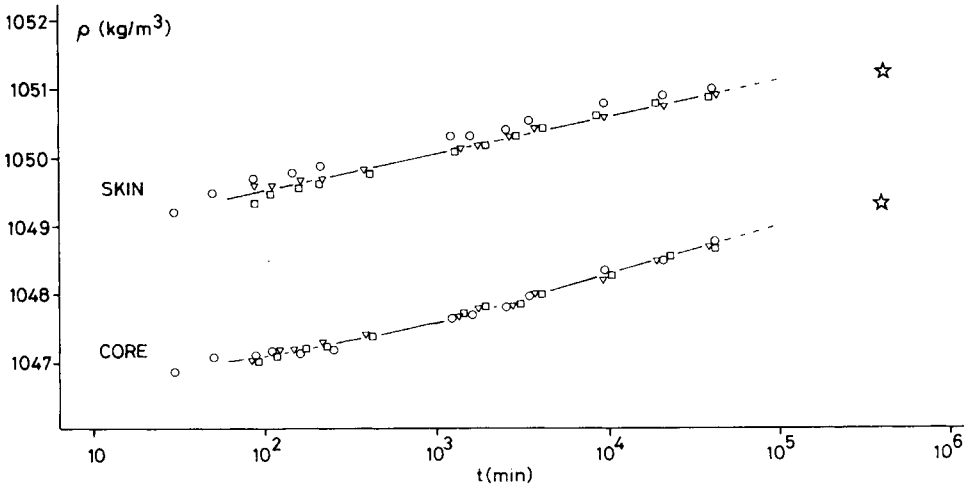

Fig. 21. Densification of skin and core material cut from a newly molded bar. Specimens cut from bars taken from the molding machine and cooled in air (▽); cooled in water (□); and cooled in liquid nitrogen (○), respectively. The densities of specimens measured after 10 months at room temperature are also shown (☆).

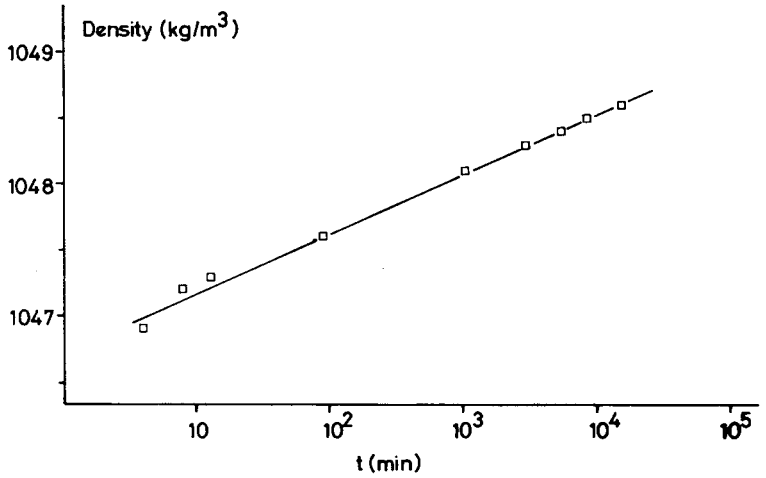

Fig. 22. Densification of specimens annealed at 110°C, cooled in air and placed in the density column at $t = 0$.

lower density (skin ~ 1049 kg/m^3, core < 1047 kg/m^3) but densified steadily in the column (Fig. 21). Some bars used in this investigation were cooled at different rates on removal from the injection molding machine (in air, in water, and in liquid nitrogen, respectively), but no difference in density could be detected either in skin or core samples. Specimens which were permitted an extended period of aging in air before being introduced into the column gave density readings identical to those found with specimens which aged in the column. In another experiment samples were annealed at 110°C for 5 h, cooled in air, and then placed in the column. Skin and core samples gave identical results with an initial reading less than 1047 kg/m^3, and then showed densification linear with log (time), climbing to approximately 1048.6 kg/m^3 in a week (Fig. 22).

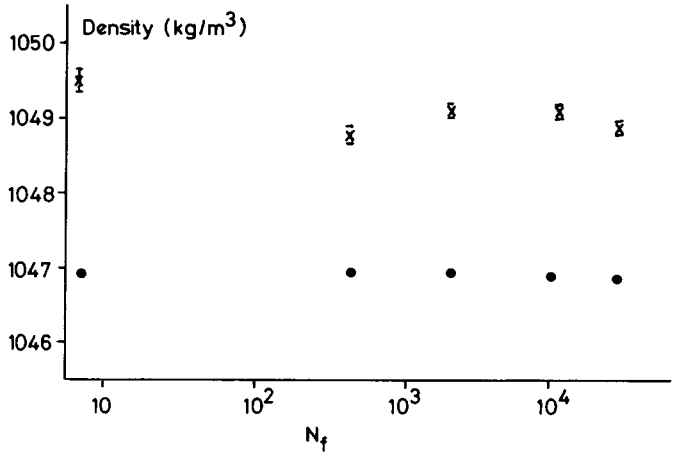

Fig. 23. Density of skin (×) and core (●) samples cut from fatigue fractured specimens that failed after N_f cycles.

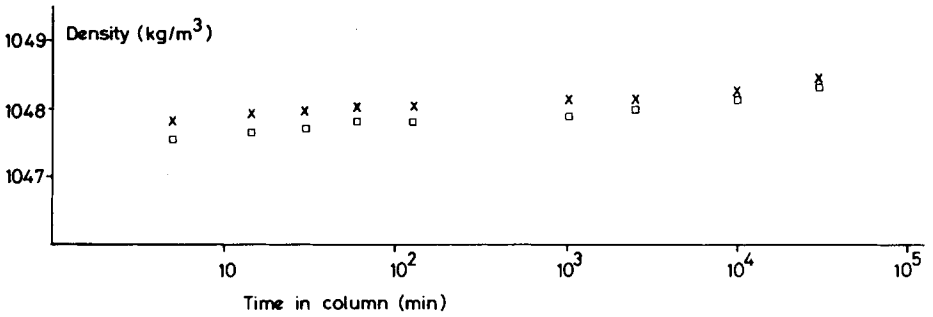

Fig. 24. Density as a function of time in the column of specimens with a high craze density (□) and a low craze density (×), respectively.

Density measurements on skin and core samples taken from bars after the completion of fatigue tests are shown in Figure 23. Five or six skin and two or three core samples were taken from each bar. The results are plotted as a function of the number of cycles to failure of the bars from which the specimens were cut. The core samples show no difference, but some variation seems to be present with the skin samples. It is possible that this amount of variation may be caused by the presence of small crazes occurring in a nonuniform manner within a single bar and with different population densities in different bars. (Recall that it was noted earlier that crazes formed in the skin on cyclic loading.) The presence of crazes was shown by a separate experiment to cause a decrease in density. Figure 24 shows the measurements made on two samples cut from the same bar, one having a high craze density

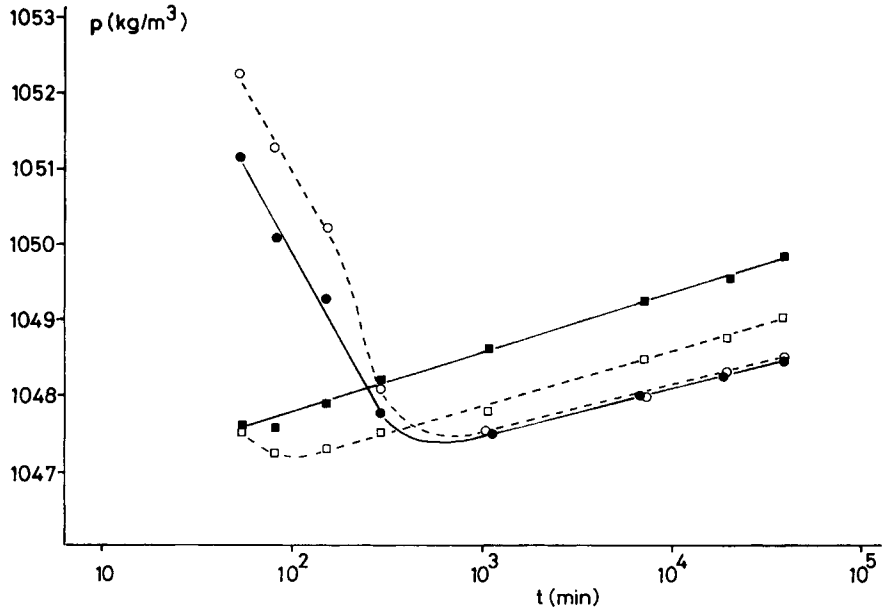

Fig. 25. Density of skin (●, ○) and core (■, □) samples taken from bars molded with an injection pressure of 62 MPa (○, □) and 186 MPa (●, ■) after prolonged storage at −85°C, plotted as a function of time after removing from the cold cabinet.

and the other being almost free from crazes on visual inspection. Both samples showed some densification, with the more densely crazed specimen increasing more rapidly, suggesting a possible contribution from (diffusion-controlled) void filling within the crazes.

Finally, specimens were taken from the skin and core of moldings prepared immediately after removing the bars from storage at −85°C. The results are plotted in Figure 25 and show that the skin samples started with a high density which dropped rapidly over the first 5 h. Regrettably results could not be obtained for times shorter than ~ 1 h because the time was required to prepare the specimens and to allow them to settle in the column. After ~ 10 h the specimens began to densify slowly, approximately linearly with log (time). This curious behavior was displayed by specimens molded at both 62 and 186 MPa. Core specimens had a lower density than the skin specimens at the beginning. There is an indication that the core density fell at very short times ($\leq$ 1 h), but in the absence of reliable measurements at shorter times this cannot be certain. For times greater than 2 h the core specimens densified linearly with log (time), becoming more dense than the skin specimens before the skin specimens began to densify.

DISCUSSION

The major purpose of the studies described here was to identify the fabrication-related aspects of fatigue failure in injection-molded PS bars. As such it resembles earlier studies by Mandell, Smith, and Huang on polysulfone[30] and Sandilands and White on poly(4-methyl pentene-1).[12] Residual stress measurements were made to investigate whether any influence of residual stresses over fatigue crack propagation rate could be detected. In fatigue failure it is inevitable that the fatigue crack will move into regions which have suffered progressively more load cycles, and it was necessary to investigate what effect cyclic loading had on the residual stress distribution. Measurements on cyclically loaded unnotched samples showed that the residual stresses did not become much altered during the fatigue tests. The fatigue crack propagation rate data from samples having different residual stress distributions did not show that residual stresses exercised a controlling influence. A modest effect cannot be ruled out because the results show significant scatter, which fractographic studies indicated may be connected with the curvature of the crack front.

The visual observations and fractographic studies revealed an apparent influence of fabrication on fatigue behavior, however, for fatigue crack initiation was found to be in specific locations, relating to features common to many injection molded articles. When unnotched bars were cyclically loaded, crazes were seen to form near the corners at low strain amplitudes or at sites 1–2 mm from the edge (and hence fairly close to, but not within, the skin) at higher strain amplitudes. In the case of low strain amplitudes, craze nucleation was always along one particular corner of the bar section at which was located a flash line which was just visible on close inspection. When unnotched specimens were cycled to failure at low strain amplitudes, it was from such sites that the final fracture started. The nucleation points at high strain amplitudes were equally easy to identify visually during running and subse-

quently in the SEM on examining the fracture surface. In many tests at high cyclic strain, nucleation appeared to have occurred at a foreign particle, but there is no obvious reason why foreign particles should locate preferentially at such positions (1–2 mm from the edge). In some cases crack nucleation took place at a similar position but without any evidence for the presence of such a stress concentrating flaw.

The observations relating to initiation may be important, because the fatigue life was found to be sensitive to specimen condition, with annealed/aged specimens giving lifetimes below those defining the S–N curve for unaged specimens. This, coupled with the failure to find any strong dependence of fatigue crack propagation rate on specimen condition, indicates that initiation plays an important part in determining fatigue life and that initiation may be controlled partly by fabrication or post fabrication conditioning.

In a separate series of tests the birefringence fell continuously during stress relaxation, indicating progressive alignment of phenyl groups (Fig. 7). Cyclic loading showed a similar effect (Fig. 8). It should be noted that the rate of change of birefringence showed a strong dependence on the stress range and that the time-dependent negative (orientation-related) difference between specimens tested at different stress amplitudes exceeded the instantaneous positive (stress optical effect) difference within a small number of hours. A similar "cross-over" effect was observed previously during stress relaxation of PS.[16]

It is now possible to offer an explanation for the relationship between the birefringence remaining after failure and the number of cycles to failure shown in Figure 9. Let us suppose that to a first approximation the time-dependent change in birefringence is proportional to the stress σ. Since birefringence also changes almost linearly with log N, then after N_f cycles the change in birefringence will be taken to be proportional to $\sigma \log N_f$. On unloading, the stress optical component is removed, and the birefringence can be described approximately by an expression of the form

$$\Delta n = -A - a\sigma \log N_f \tag{6}$$

where A and a are both positive. The as-molded birefringence, $-A$, is negative with PS injection moldings as a consequence of molecular orientation. By taking corresponding pairs of values of σ and log N_f from the S–N curve in Figure 5, eq. (6) can be used to generate the form of the relationship between Δn and log N_f at the end of the fatigue tests (Fig. 26). It is seen to resemble the experimental curve in Figure 9.

Finally, the results on the variation of density on aging merit attention. Since the polymer cools rapidly through the glass transition temperature during injection molding, it is not surprising that the material solidifies into a nonequilibrium state and that post-molding densification takes place on aging. That the as-molded skin is denser than the core is also to be expected because the skin material sets at a high pressure (while the injection system pressure is still being delivered into the cavity), whereas the core material sets at a lower pressure after the gate has frozen, decoupling the cavity from the injection system. Molecular orientation would generally permit closer molecular packing, thus favoring a higher skin density. The densification of the material that takes place on aging correlates with the progressive increase in stiffness seen

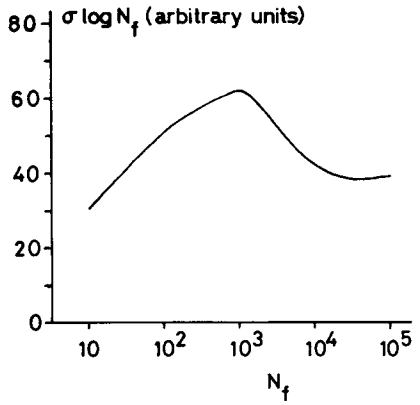

Fig. 26. Plot of $\sigma \log N_f$ (in arbitrary units) vs. $\log N_f$ using Figure 5.

in the tensile tests (Fig. 10). The strange density behavior shown by specimens cut from a bar after prolonged storage at −85°C is quite important. The core density is at its lowest value after ~ 1 h, only a short time after the timing of the tensile tests. This correlates with the low stiffness measured with specimens in this state. The rapid changes in density, which are different in the skin and core, will inevitably correspond to changes in the linear dimensions in the xy plane and will cause changes in the residual stress. This may explain why the results of the residual stress analysis for bars stored at −85°C and tested as soon as room temperature equilibrium was restored were anomalous. Changes in the residual stress distribution corresponding to the density changes will be occurring throughout the execution of the layer removal procedure, which takes ~ 3 h. During low temperature storage the density changes which must occur (as evidenced by the high skin density measured a short time after removing the material from the cold cabinet) will modify the residual stress distribution. The kinetics of densification of the material during storage at low temperature and the subsequent time-dependent recovery at room temperature need to be examined more closely.

CONCLUSIONS

The fatigue crack propagation rate in PS injection moldings has been found to be fairly insensitive to molding conditions or post-molding conditioning (low temperature storage, annealing, cyclic loading prior to notching). Aging for long periods or annealing at elevated temperature produced a shorter fatigue life, indicating that the initiation process had probably been influenced. The site of initiation in unnotched specimens tested at high strain amplitudes was on the central (xy) plane of the bar, 1–2 mm from one edge, a similar position to that obtained in uniaxial tensile tests. With low strain amplitudes the site of initiation was near one corner.

The presence of residual stresses would be expected to have at most a secondary influence on the fatigue crack propagation rate because the stresses must balance over the total cross section, and any tendency for the rate to increase in tensile regions would be at least partly compensated by the retarding effect of compressive stresses elsewhere. The shape of the crack front might be influenced by the residual stresses, but, more importantly, they

might influence the site of initiation. There seem to be other factors involved, however, and it is suspected that the skin/core morphology exercises some control over the behavior. This could arise in several ways. If the skin and core have different stiffnesses, then on applying a uniaxial deformation strong shear stresses will develop at the skin/core boundary. Similarly, if the skin and core have different thermal expansion coefficients, then on changing the temperature shear stresses will form at the boundary. The fracture surfaces showed a distinct skin/core morphology which may be the consequence primarily of the different strengths of the two regions. Further work is needed to properly define the physical properties of the skin and core material.

Finally, prolonged residence at $-85°C$ produced significant property changes, contrary to expectations. This behavior requires further examination and explanation.

The financial support of SERC is gratefully acknowledged.

References

1. B. Haworth, C. S. Hindle, G. J. Sandilands, and J. R. White, *Plast. Rubber Process. Appl.*, **2**, 59 (1982).
2. L. D. Coxon and J. R. White, *Polym. Eng. Sci.*, **20**, 230 (1980).
3. B. Haworth and J. R. White, *J. Mater. Sci.*, **16**, 3263 (1981).
4. P. S. Allan and M. J. Mortazavi, *Plast. Rubber Process. Appl.*, **5**, 71 (1985).
5. D. P. Russell and P. W. R. Beaumont, *J. Mater. Sci.*, **15**, 208 (1980).
6. M. Thompson and J. R. White, *Polym. Eng. Sci.*, **24**, 227 (1984).
7. M. M. Qayyum and J. R. White, *J. Mater. Sci.*, **20**, 2557 (1985).
8. R. W. Hertzberg and J. A. Manson *Fatigue of Engineering Plastics*, Academic, New York, London, 1980.
9. J. R. White, *Polym. Testing*, **4**, 165 (1984) (also in *Measurement Techniques for Polymeric Solids*, Eds., R. P. Brown and B. E. Read, Elsevier, Barking, U. K., 1984, Chap. 8).
10. R. G. Treuting and W. T. Read, Jr., *J. Appl. Phys.*, **22**, 130 (1951).
11. G. J. Sandilands, Ph.D. thesis, University of Newcastle upon Tyne, 1983.
12. G. J. Sandilands and J. R. White, *J. Appl. Polym. Sci.*, **30**, 4771 (1985).
13. A. I. Isayev and T. Hariharan, *Polym. Eng. Sci.*, **25**, 271 (1985).
14. J. R. White, *J. Mater. Sci.*, **20**, 2377 (1985).
15. G. J. Sandilands and J. R. White, *Polymer*, **21**, 338 (1980).
16. M. M. Qayyum and J. R. White, *Polymer*, **23**, 129 (1982).
17. A. V. Iacopi, M.Sc. thesis, University of Newcastle upon Tyne, 1984.
18. P. Beahan, M. Bevis, and D. Hull, *Polymer*, **14**, 96 (1979).
19. P. Beahan, M. Bevis, and D. Hull, *Proc. Roy. Soc. London*, **A343**, 525 (1975).
20. J. A. Sauer, A. D. McMaster, and D. R. Morrow, *J. Macromol. Sci. Phys.*, **B12**, 535 (1976).
21. M. D. Skibo, R. W. Hertzberg, and J. A. Manson, *J. Mater. Sci.*, **11**, 479 (1976).
22. A. V. Iacopi and J. R. White, *J. Appl. Polym. Sci.*, (Paper II), 607–623
23. J. G. Williams, *Stress Analysis of Polymers*, Ellis Horwood, Chichester, U.K., 1980.
24. J. G. Williams *Fracture Mechanics of Polymers*, Ellis Horwood, Chichester, U.K., 1984.
25. A. J. Kinloch and R. J. Young, *Fracture Behaviour of Polymers*, Applied Science, Barking, U.K., 1983.
26. P. J. Hine, R. A. Duckett, and I. M. Ward, *Polymer*, **22**, 1745 (1981).
27. J. Hoare and D. Hull, *J. Mater. Sci.*, **10**, 1861 (1975).
28. D. L. G. Lainchbury and M. Bevis, *J. Mater. Sci.*, **11**, 2222 (1976).
29. P. Colclough, J. N. Hay, and N. Walker, *J. Polym. Sci. Polym. Lett.*, Ed., **16**, 591 (1978).
30. J. F. Mandell, K. L. Smith, and D. D. Huang, *Polym. Eng. Sci.*, **21**, 1173 (1981).

Received November 12, 1985
Accepted April 21, 1986